



Boosting HER Performance of Pt-Based Catalysts Immobilized on Functionalized Vulcan Carbon by Atomic Layer Deposition

Wei Luo[†], Jie Gan[†], Zikun Huang, Wenyao Chen^{*}, Gang Qian, Xinggui Zhou and Xuezhi Duan^{*}

State Key Laboratory of Chemical Engineering, East China University of Science and Technology, Shanghai, China

OPEN ACCESS

Edited by:

Zhonghua Xiang,
Beijing University of Chemical
Technology, China

Reviewed by:

Yuen Wu,
University of Science and Technology
of China, China
Yongquan Qu,
Xi'an University, China

*Correspondence:

Wenyao Chen
wenyao.chen@mail.ecust.edu.cn
Xuezhi Duan
xzduan@ecust.edu.cn

[†]These authors have contributed
equally to this work

Specialty section:

This article was submitted to
Energy Materials,
a section of the journal
Frontiers in Materials

Received: 27 August 2019

Accepted: 23 September 2019

Published: 09 October 2019

Citation:

Luo W, Gan J, Huang Z, Chen W,
Qian G, Zhou X and Duan X (2019)
Boosting HER Performance of
Pt-Based Catalysts Immobilized on
Functionalized Vulcan Carbon by
Atomic Layer Deposition.
Front. Mater. 6:251.
doi: 10.3389/fmats.2019.00251

Development of cost-effective Pt-based electrocatalysts is of scientific and industrial importance for hydrogen evolution from water splitting. In this work, cost-efficient Pt-based catalysts, immobilized on functionalized Vulcan Carbon (VC) from hydrothermal treatment of Ru precursor and ethylene glycol solution, for hydrogen evolution reaction (HER) are elaborately constructed via an elegant and controllable atomic layer deposition (ALD) technique. More carboxyl groups on the functionalized VC are suggested as the anchor sites for Pt immobilization, which gives rise to the more Pt active sites, desirable Pt electronic properties and stronger Pt-support interaction. The resultant 7.1 wt% Pt-based composite catalyst exhibits remarkably boosted HER activity and stability than the commercial 20% Pt/C catalyst. These insights could open up a new avenue for fabrication of cost-effective Pt/C HER catalysts based on ALD technique.

Keywords: hydrogen evolution reaction, Pt-based catalysts, functionalized Vulcan Carbon, atomic layer deposition, cost-effective

INTRODUCTION

Electrocatalytic hydrogen evolution reaction (HER) in water splitting has been recently identified as an economical and sustainable method for H₂ production (Li et al., 2011; Shi and Zhang, 2016; Lyu et al., 2017; Ouyang et al., 2017; Seh et al., 2017). Hitherto, Pt-based catalysts are considered as the state-of-the-art choice for catalyzing HER under acidic conditions, because Pt sits very near the top of the volcano (Skúlason et al., 2010; Chao et al., 2017; Seh et al., 2017; Jiang et al., 2018; Wang et al., 2018). Limited by its expense and scarcity for large-scale commercialization, one strategy to increase the Pt utilization efficiency is reducing the Pt particle size toward the increased Pt dispersion and thus more Pt active sites (Zheng et al., 2015; Anantharaj et al., 2016; Cheng et al., 2016; Qu et al., 2019), and another strategy is tailoring the Pt electronic properties toward the enhanced intrinsic activity (Greeley et al., 2006; Li et al., 2018, 2019). Although the conductive carbon supports endow the Pt-based catalysts with an effective electron transfer system, their low interaction with the supported metal nanoparticles requires the pre-functionalization of the carbon supports to stabilize the metal nanoparticles toward stable HER performance (Ryndin et al., 1981; Kitchin et al., 2004; Marichy et al., 2012; Hou et al., 2015; Cheng et al., 2016; Anantharaj et al., 2017; Qu et al., 2019).

Recently, atomic layer deposition (ALD) has gained considerable attentions for the well-controlled synthesis of carbon supported Pt-based catalysts, because it can precisely control

the size of Pt nanoparticles (George, 2009; Gao and Qin, 2017). For such technique, it proceeds via the self-limiting surface reactions, i.e., the precursor reacting with the surface functional groups on the substrate. To this end, there are an amount of studies about the surface treatments to introduce more surface functional groups for anchoring the Pt species and the increased cycles to obtain relatively high Pt loading, but to cause the loss of the Pt active sites because of the increased Pt particle size (Liu et al., 2009; Li et al., 2010; Zhang et al., 2017). As far as we know, only limited study on the ALD-synthesized Pt/C catalysts, being highly active (i.e., the 16 mA cm^{-2} of current density at the overpotential of 0.05V) and stable (i.e., the 4% loss of its initial current density after 1000 CV cycles), has been conducted for the HER (Cheng et al., 2016). As a consecutive effort, more studies are highly desirable to gain in-depth understanding of ALD-synthesized Pt/C catalyzed HER and rationally design cost-effective and stable Pt/C HER electrocatalysts.

In this work, cost-effective Pt-based composite catalysts immobilized on functionalized Vulcan Carbon (VC) were fabricated for the HER. The functionalization of VC was carried out via hydrothermal treatment in Ru precursor and ethylene glycol solution to create abundant surface functional groups for Pt immobilization by the ALD technique. The resultant Pt/Ru/VC composite catalyst together with the referenced Pt/VC, Ru/VC and commercial 20 wt% Pt/C catalysts were tested and characterized by multiple techniques such as HAADF-STEM, HRTEM, XPS, and TGA. Finally, the relationship between the catalyst structure and performance was established.

EXPERIMENTAL SECTION

Catalyst Preparation

The Ru/VC catalyst was synthesized by hydrothermal treatment of Ru precursor and ethylene glycol solution. Typically, 0.6 g urea (Sinopharm Chemical Reagent Co., Ltd) was dissolved in 20 mL ultrapure water, then 0.5 g Vulcan Carbon (VC, Sigma-Aldrich Co., Ltd) was added into the solution under ultrasonication for 30 min. The as-obtained suspension was mixed with 2.23 mL aqueous RuCl_3 (Adamas Reagent Co., Ltd) solution with the concentration of 0.04 g mL^{-1} , which was further transferred into the hydrothermal reactor. The hydrothermal reactor was kept in the oven under 90°C for 1 h before cooling down to room temperature. Afterwards, 20 mL ethylene glycol (Sigma-Aldrich Co., Ltd) was directly mixed with the solution under ultrasonication for 30 min, followed by heating to 120°C for another 1 h. Finally, the as-obtained slurry was filtered, washed and dried at 80°C overnight. For a comparison, EG-VC was prepared using the same method as described above except the addition of aqueous RuCl_3 solution, which could be employed as the reference sample.

The Pt/VC catalyst was synthesized by ALD. Typically, a certain amount of Vulcan Carbon (VC, Sigma-Aldrich Co., Ltd) was placed in a container inside the ALD reactor chamber. The Pt ALD was performed by sequential exposure of the VC to (methylcyclopentadienyl) trimethylplatinum (MeCpPtMe_3 , Strem Chemicals, 99%) and ozone (O_3) produced using an ozone generator. Nitrogen was employed as the purging and carrier

gas. The container for VC was placed inside the ALD reaction chamber. The deposition temperature was 250°C , while the temperature for the container of MeCpPtMe_3 was kept at 65°C to provide a steady state flux of MeCpPtMe_3 to the reactor. ALD pipelines were heated to 150°C to avoid precursor condensation. For each ALD cycle, the pulse, exposure, and purge time for MeCpPtMe_3 were 0.5, 12, and 25 s, while those for O_3 were 1, 12, and 25 s, respectively. Similarly, the Pt/Ru/VC and Pt/EG-VC catalysts were also synthesized by ALD, which the as-synthesized Ru/VC and EG/VC were employed as the support of Pt catalyst, respectively. For all the ALD-synthesized catalysts, the number for ALD cycle was kept as 20. Moreover, the commercial 20 wt% Pt catalyst over Vulcan XC-72 (20% Pt/C) was obtained from Sigma-Aldrich.

Catalyst Characterization

The size and distribution of these catalysts were characterized by high-angle annular dark-field scanning transmission electron microscopy (HAADF-STEM, Tecnai G2 F20 S-Twin). The mean particle sizes of catalysts were calculated based on the sizes of at least 200 random particles. The morphology of the metal particles was observed by high resolution transmission electron microscopy (HRTEM, JEOL JSM-2100). The surface composition and electronic structure of catalysts were investigated using the X-ray photoelectron spectrometer (XPS, Kratos AXIS SUPRA) equipped with an Al K_α X-ray (1486.6 eV, excitation source working at 15 kV). The C 1s peak at 284.6 eV was taken as an internal standard to correct the shift in the binding energy caused by sample charging. The inductively coupled plasma atomic emission spectrometer (Agilent 725-ES ICP-AES) was employed to measure the metal contents. Laser Micro-Raman Spectrometer (Raman, InVia Reflex, Renishaw) was employed to characterize the degree of graphitization and electronic properties for these catalysts.

Electrochemical Measurements

The electrochemical performance was tested by the three-electrode system with the CHI760E (CH Instruments Ins.) instrument. A saturated Ag/AgCl electrode and graphite rod were used as the counter and reference electrode, respectively. The working electrode was prepared by the following procedures: (1) 1 mL ethanol (Sigma-Aldrich Co., Ltd) and 30 μL Nafion 5 wt.% solution (DuPont Inc.) were firstly mixed, followed by the addition of 5 mg catalyst under ultrasonication to obtain a homogeneous ink; (2) a certain amount of catalyst ink (5 μL) was drop-casted on a glassy carbon electrode (GCE) with a diameter of 3 mm; (3) the drop-casted GCE was dried at ambient conditions under air. All data were corrected for 90% iR potential drop (R, ohmic drop $6\sim 8 \Omega$). For a saturated Ag/AgCl electrode, the potential against reversible hydrogen electrode (RHE) was calculated according to the following equation:

$$E (\text{vs. RHE}) = E (\text{vs. Ag/AgCl}) + E^0 (\text{Ag/AgCl}) + 0.0591 \times \text{pH}$$

where E (vs. RHE) is the potential vs. RHE, E (vs. Ag/AgCl) is the potential vs. Ag/AgCl and $E^0(\text{Ag/AgCl})$ is the potential of Ag/AgCl respect to the standard hydrogen electrode.

0.5 M H₂SO₄ (Sinopharm Chemical Reagent Co., Ltd) was employed as the electrolyte, which was degassed by bubbling N₂ for at least 30 min. Before the electrochemical measurements, the catalysts were activated by 20 cyclic voltammetry (CV) scans along the potential window from 0 to -0.5 V vs. RHE in 0.5 M H₂SO₄ at a scan rate of 100 mV s⁻¹, then linear sweep voltammetry (LSV) was performed with a scan rate of 5 mV s⁻¹. The electrochemical impedance spectroscopy (EIS) measurements were conducted from 100 kHz to 1 Hz. The amplitude of the sinusoidal potential signal was 5 mV. Electrochemical capacitance was measured by CV at different scan rates of 20, 40, 60, 80, 120, 160, 240, and 320 mV s⁻¹. The capacitive currents were collected within the potential window from 0.45 to 0.65 V vs. RHE where no apparent Faradaic processes were observed. These measured capacitive currents were then plotted as a function of scan rates, which the slope could be used to calculate the electrochemical capacitance. Assuming that the specific capacitance of a flat surface is ~ 40 μF for 1 cm² of real surface area, the ECSA could be estimated as:

$$ECSA = \frac{\text{specific capacitance}}{40 \mu F \text{ cm}^{-2} \text{ per cm}^2_{ECSA}}$$

The as-obtained Tafel plots were fitting into the Tafel equation:

$$\eta = a + b \log j$$

which η is the overpotential, j is the current density and b is the Tafel slope.

RESULTS AND DISCUSSION

Boosted HER Activity and Stability of Pt-Based Catalysts by ALD

The Vulcan Carbon (VC) was functionalized by hydrothermal treatment in aqueous RuCl₃ and EG solution, which was used to immobilize Pt nanoparticles by the ALD method. The as-prepared Pt-based catalyst (i.e., Pt/Ru/VC), together with the ALD-synthesized Pt catalyst over the pristine VC support (i.e., Pt/VC), functionalized VC (i.e., Ru/VC), and commercial 20 wt% Pt/C catalysts, was characterized by HAADF-STEM measurements to obtain the reliable size and distribution of metal nanoparticles. As can be clearly seen in **Figures 1A–C**, the former three catalysts exhibit relatively homogeneous distribution of metal particles, especially for the ALD-synthesized catalysts. The average metal particle sizes based on the measurements of more than 200 random particles were determined to be 1.5 ± 0.4, 1.6 ± 0.1, and 1.7 ± 0.3 nm for the Pt/Ru/VC, Pt/VC, and Ru/VC catalysts, respectively. Hence, these three catalysts exhibit similar size and distribution of metal particles, which would help to minimize the size effects and make a fair comparison on the catalytic activities for the HER (Gomez et al., 1993; Durst et al., 2014). On the contrary, as shown in **Figure 1D**, the commercial 20 wt% Pt/C catalyst exhibits remarkable Pt aggregates in specific areas, possibly due to the high Pt loading and easy migration of Pt particles. As a result, the wider distribution of Pt particles is

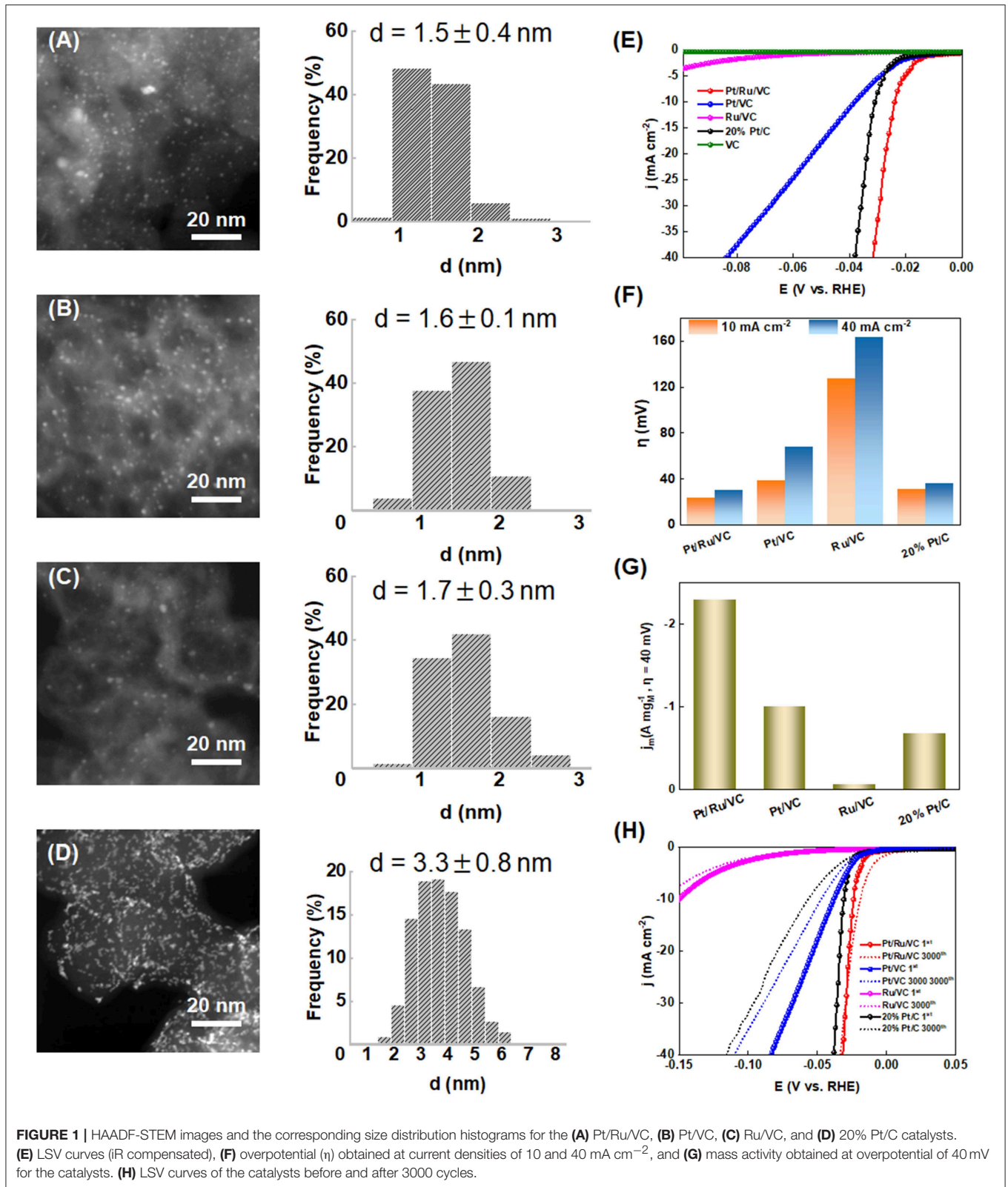
observed, and the average Pt particle size is determined to be 3.3 ± 0.8 nm. Hence, the as-prepared three catalysts exhibit smaller metal particle sizes and narrower size distributions than the commercial 20 wt% Pt/C catalyst, making them good candidates for the HER.

To obtain their HER performances, these catalysts were evaluated by LSV measurements in acid media, and the results are shown in **Figures 1E,F**. Interestingly, the Pt/Ru/VC catalyst is observed to generate a 10 mA cm⁻² current density at a very low overpotential of 23 mV, where such current density is comparable to solar fuel synthesis (Zeng and Li, 2015; Li et al., 2018). To achieve the current density of 40 mA cm⁻², the Pt/Ru/VC catalyst still delivers a low overpotential of 30 mV. In comparison, as shown in **Table S1**, the other two catalysts together with the commercial 20 wt% Pt/C catalyst exhibit higher overpotentials, especially for the Ru/VC catalyst. Specifically, the Ru/VC catalyst exhibits the overpotential of 127 mV at 10 mA cm⁻² and 163 mV at 40 mA cm⁻². These results demonstrate the outstanding HER activity of our developed Pt/Ru/VC composite catalyst.

Furthermore, the mass activities of these catalysts were compared, which were determined by normalizing the current densities at 40 mV potential to the total mass of metal species. As obviously shown in **Figure 1G**, the mass activity of the Pt/Ru/VC catalyst is up to 2.3 A mg_M⁻¹ at the 40 mV overpotential, which is 3.3, 2.3, and even 23 times higher than that of the 20% Pt/C, Pt/VC, and Ru/VC catalyst, respectively. Apart from the catalytic activities, the stability is another important criterion for the Pt-based catalysts in consideration of their high cost and limited abundance. To this end, the stability of these catalysts was evaluated by CV measurements in the potential range from 0.1 to -0.25 V vs. RHE for 3000 cycles. As shown in **Figure 1H** and **Table S1**, the commercial 20 wt% Pt/C catalyst shows the largest negative shift of the polarization curve by nearly 26 mV at 10 mA cm⁻² after the 3000 cycles, indicating the lowest catalyst stability, while the Pt/VC catalyst displays the smaller negative shift of 11 mV at 10 mA cm⁻². Unexpectedly, the Pt/Ru/VC catalyst almost shows no negative shift after the 3000 cycles. Based on the above results, the monometallic Pt catalyst exhibits much higher HER activity and stability than the monometallic Ru catalyst, and the Pt/Ru/VC catalyst appears to be the best catalyst for HER with the highest activity and stability. This suggests that the Pt is more active than the Ru, and the Pt over the Pt/Ru/VC composite catalyst most likely acts as the dominant active species for the HER.

The Crucial Role of the Functionalized VC for the Pt-Based Catalysts

ICP-AES measurements were first carried out to compare the difference in the metal loadings of these catalysts for understanding the significantly enhanced activity and stability of the Pt/Ru/VC composite catalyst. As shown in **Figure 2A**, the Pt and Ru loadings for the Pt/VC and Ru/VC catalysts are determined to be 3.2 and 2.1 wt%, respectively. In comparison, for the Pt/Ru/VC catalyst, the Pt loading exhibits a dramatic increase up to 7.1 wt%. This strongly suggests that the promoting



role of the functionalized VC on the deposition of Pt particles. Furthermore, from the point view of the structural effects, influences of the metal loadings on the HER activities were

investigated based on the CV curves in **Figure S1**, where the electrochemical double-layer capacitance (C_{dl}) was used to determine the electrochemically active surface area (ECSA)

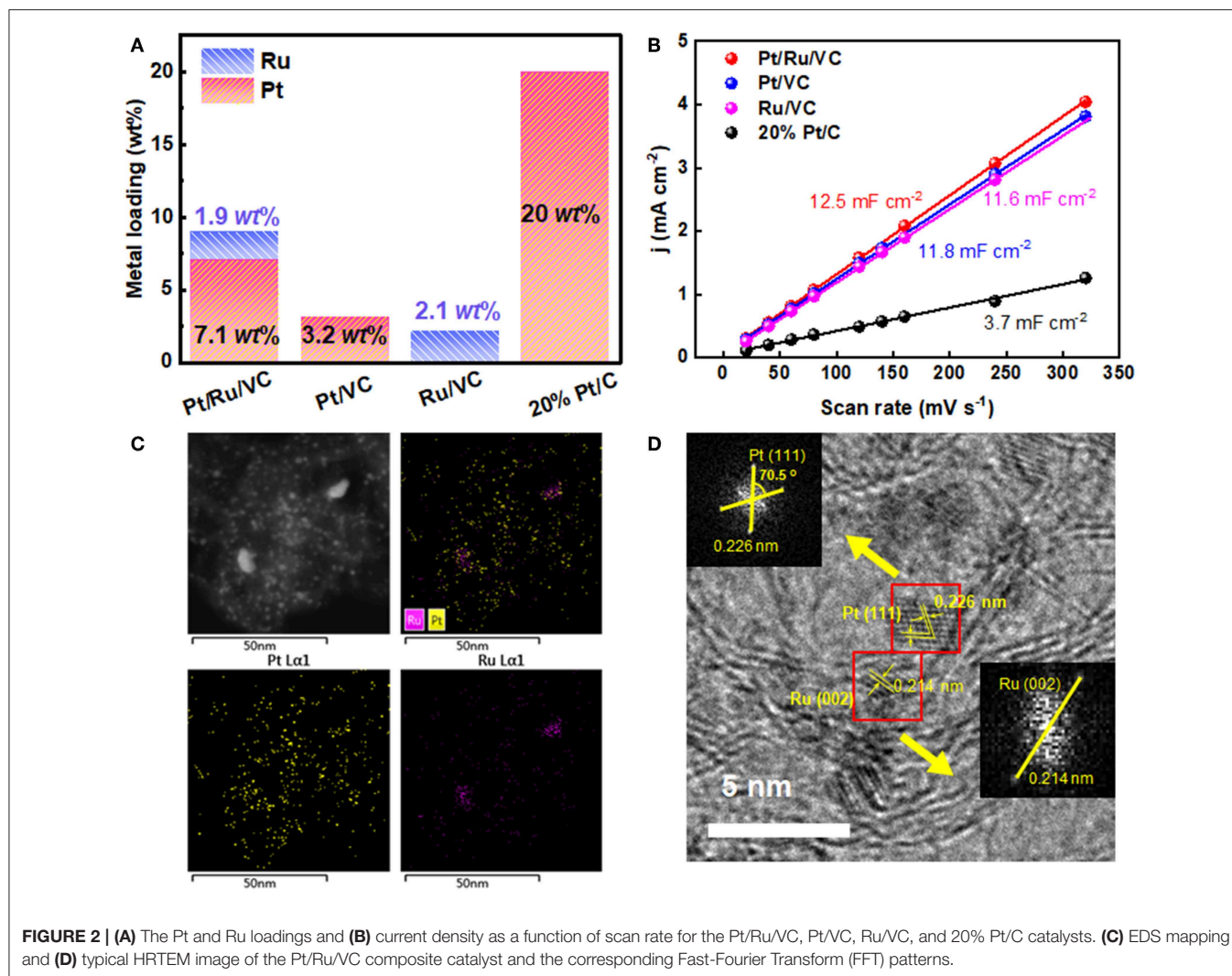


FIGURE 2 | (A) The Pt and Ru loadings and **(B)** current density as a function of scan rate for the Pt/Ru/VC, Pt/VC, Ru/VC, and 20% Pt/C catalysts. **(C)** EDS mapping and **(D)** typical HRTEM image of the Pt/Ru/VC composite catalyst and the corresponding Fast-Fourier Transform (FFT) patterns.

(Durst et al., 2014; Li et al., 2018). As shown in **Figure 2B**, the ECSA for the Pt/Ru/VC, Pt/VC, Ru/VC, and commercial 20% Pt/C catalysts is determined to be 12.5, 11.8, 11.6, and 3.7 mF cm^{-2} , respectively. As expected, the Pt/Ru/VC composite catalyst, having the small sized Pt nanoparticles with the relatively high Pt loading, exhibits the largest ECSA, which would provide a rational interpretation for its highest activity.

To gain more insights into the microstructural properties of the Pt/Ru/VC composite catalyst, the EDS mapping was conducted to characterize the distribution of Pt and Ru over such catalyst. As shown in **Figure 2C**, it can be seen that both Pt and Ru homogeneously distribute across the VC surface, together with few Ru aggregates. Considering the small size of metal particles and the detected limitation of EDS mapping, it is difficult to determine the fine structure and composition of metal particles, e.g., alloy, core-shell, or monometallic mixtures. Hence, HRTEM was further employed to characterize the microstructure of this catalyst, and the results are shown in **Figure 2D**. Apparently, the catalyst exhibits continuous lattice fringes across the VC surface, which could be ascribed to the

Pt and/or Ru nanoparticles. To obtain more information, Fast-Fourier Transform (FFT) of the selected two particles was conducted in **Figure 2D**. Correspondingly, the spacings of the crystal lattices were determined to be 0.226 and 0.214 nm, which could be attributed to the Pt(111) and Ru(001) facets, respectively. Therefore, based on the above observations, in most cases, the Pt and Ru nanoparticles separately distribute instead of forming alloy across the VC surface.

It is well-known that not only the structural properties but also electronic properties have significant influences on the HER performance. Hence, the electronic properties of these catalysts were characterized and compared by XPS. As shown in **Figure 3A**, all the catalysts exhibit Pt 4f doublets, which could be deconvoluted into Pt^0 , Pt^{2+} , and Pt^{4+} based on the binding energies. It is worth to note that the metallic Pt has been identified as the main active species for the HER, and thus selected as the indicator of their electronic properties (Seh et al., 2017). It can be seen that the metallic Pt dominates Pt species for these catalysts, while the corresponding binding energy, i.e., Pt^0 4f_{7/2}, follows an order of Pt/Ru/VC (72.0 eV) > Pt/VC (71.7 eV) > commercial

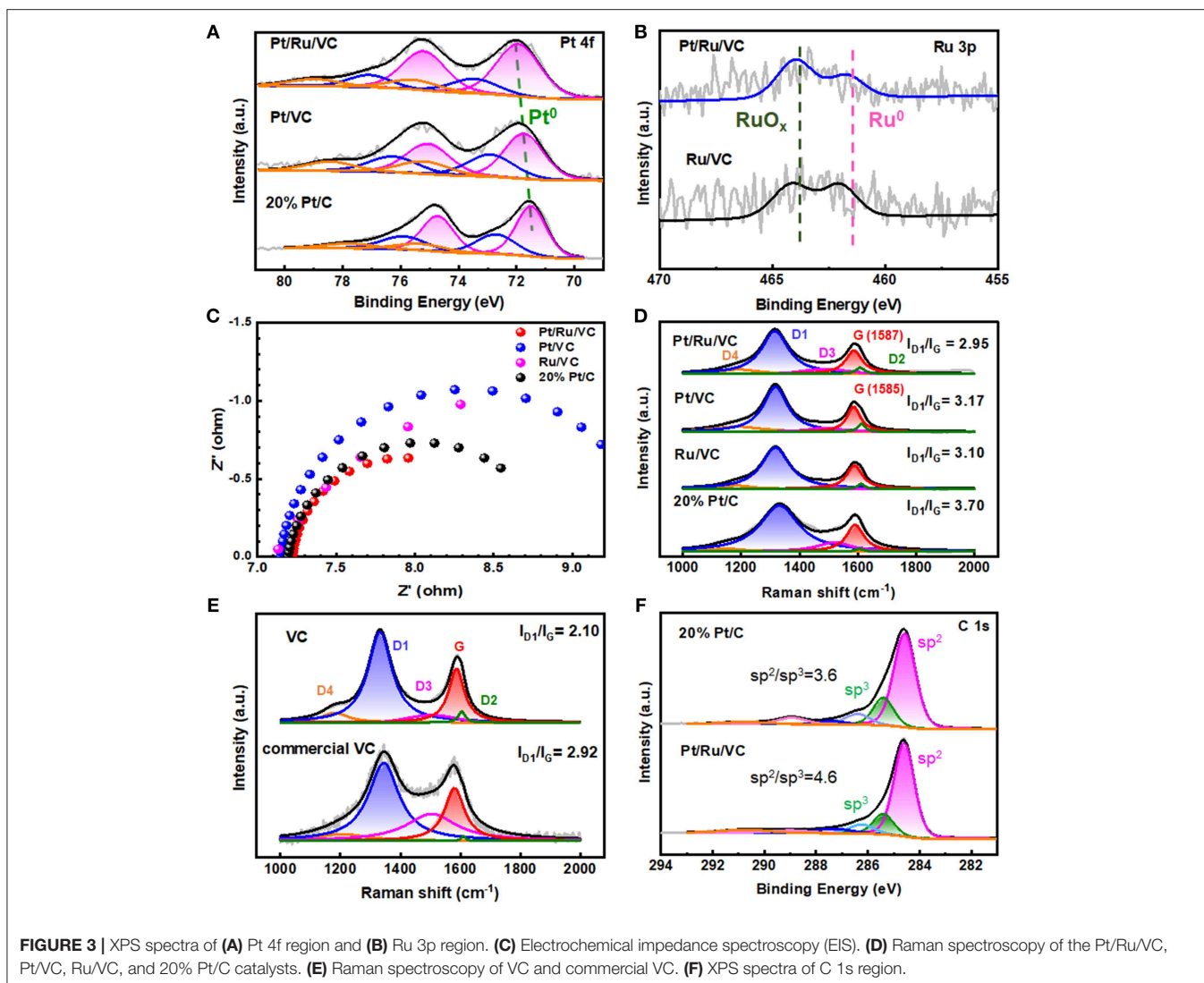


FIGURE 3 | XPS spectra of (A) Pt 4f region and (B) Ru 3p region. (C) Electrochemical impedance spectroscopy (EIS). (D) Raman spectroscopy of the Pt/Ru/VC, Pt/VC, Ru/VC, and 20% Pt/C catalysts. (E) Raman spectroscopy of VC and commercial VC. (F) XPS spectra of C 1s region.

20 wt% Pt/C (71.5 eV). Interestingly, this trend of Pt 4f binding energy is highly consistent with that of the corresponding mass activity in **Figure 1G** for this reaction, suggesting that the higher Pt 4f binding energy favors the HER. Moreover, based on the XPS Ru 3p spectra in **Figure 3B**, the deconvolution results indicate that the content of metallic Ru within the Pt/Ru/VC catalyst is much less than that of the Ru/VC catalyst, reasonably assuming that the ALD could promote the oxidation of Ru and in turn facilitate the deposition of Pt particles over the catalyst. Therefore, it could be deduced that the highest Pt⁰ 4f binding energy is another important factor for the Pt/Ru/VC catalyst with the highest HER activity.

Moreover, considering that the HER performance is also affected by electron conductivity of catalyst, it is investigated by the EIS for these catalysts (Zhu et al., 2018). As shown in **Figure 3C**, it is found that the Pt/Ru/VC composite catalyst has the smallest charge-transfer resistance among these catalysts, indicating the fastest electron transfer rate in the reaction kinetics

at the interface between electrocatalyst and electrolyte. To obtain more details about the electron transfer, Raman measurements were further carried out for these catalysts. Considering that Raman scattering is strongly sensitive to the electronic properties of carbon-based catalysts, the G band shifts could originate from the electron transfer between metal and support (Sgobba and Guldi, 2009; Dennany et al., 2010; Yin et al., 2018). As shown in **Figure 3D**, compared with the Pt/VC, the Pt/Ru/VC exhibits an upshift of 2 cm⁻¹ in the G band, consistent with its higher Pt 4f binding energy. Moreover, it can be also seen in **Figure 3D** that the Pt/Ru/VC composite catalyst shows a higher degree of graphitization with the smallest I_{D1}/I_G (2.95) than the Pt/VC (3.17), Ru/VC (3.10), and commercial 20% Pt/C catalysts (3.70). Obviously, the trend of graphitization degree agrees well with that of the above EIS values, which the higher graphitization degree would be more beneficial for electron transfer. Therefore, the highest electron conductivity of the Pt/Ru/VC composite catalyst could also contribute to its highest HER activity.

To verify this idea, another type of VC (i.e., commercial VC), as the support of commercial 20 wt% Pt/VC catalyst, was purchased and also characterized by Raman spectroscopy, thus excluding the metal effects. As shown in **Figure 3E**, the commercial VC exhibits a higher I_{D1}/I_G (2.92) than the VC (2.10) used in this study. Hence, the graphitization degree of the VC is still higher than that of commercial VC regardless of metal deposition. Moreover, the XPS C 1s spectra in **Figure 3F** shows that the Pt/Ru/VC composite catalyst exhibits higher $C(sp^2)/C(sp^3)$ of 4.6 than that of 3.6 for the commercial 20% Pt/C catalyst. Considering that electron conductivity of $C(sp^2)$ is much higher than that of $C(sp^3)$ (Li et al., 2010; Zhu et al., 2015), the Pt/Ru/VC composite catalyst with more $C(sp^2)$ should possess higher electron conductivity, which is still consistent with the results from Raman spectroscopy. Therefore, the Pt/Ru/VC composite catalyst appears to have the highest electron conductivity toward high HER activity.

Tafel behaviors for these catalysts were further studied to reveal the electrochemical kinetics and reaction mechanism for

HER. It can be seen in **Figure 4A** that both the Pt/Ru/VC and commercial 20% Pt/C catalysts show the lowest Tafel slope (30.6 mV/dec), compared with the Pt/VC (132.8 mV/dec), and Ru/VC catalysts (86.7 mV/dec). According to Butler-Volmer kinetics, the change in Tafel slopes indicates the transition between two reaction pathways, i.e., Volmer-Tafel and Volmer-Heyrovsky mechanism (Zeng and Li, 2015). Specifically, the Tafel slope of 118, 39, and 29.5 mV/dec could be, respectively, classified into discharge reaction (Volmer step), electrochemical desorption reaction (Heyrovsky step) and recombination reaction (Tafel step) as the rate-determine steps (RDS) (Zeng and Li, 2015). As shown in **Figure 4B**, the Tafel slope is determined to be 30.6, 132.8, 86.7, and 30.6 mV/dec for the Pt/Ru/VC, Pt/VC, Ru/VC, and commercial 20 wt% Pt/C catalysts, respectively. Hence, the Pt/Ru/VC composite catalyst with the highest Pt 4f binding energy can have the strongest hydrogen adsorption, resulting in the Tafel step as the RDS. On the contrary, Pt/VC with lower Pt 4f binding energy could exhibit weaker adsorption of hydrogen, corresponding to the Volmer step as the RDS.

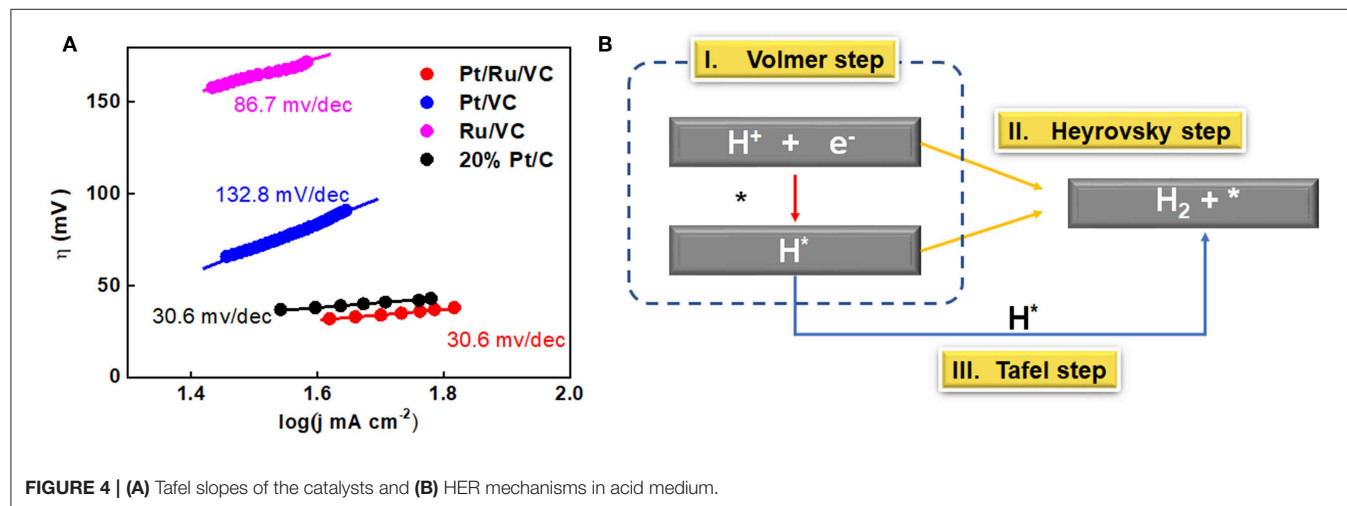


FIGURE 4 | (A) Tafel slopes of the catalysts and **(B)** HER mechanisms in acid medium.

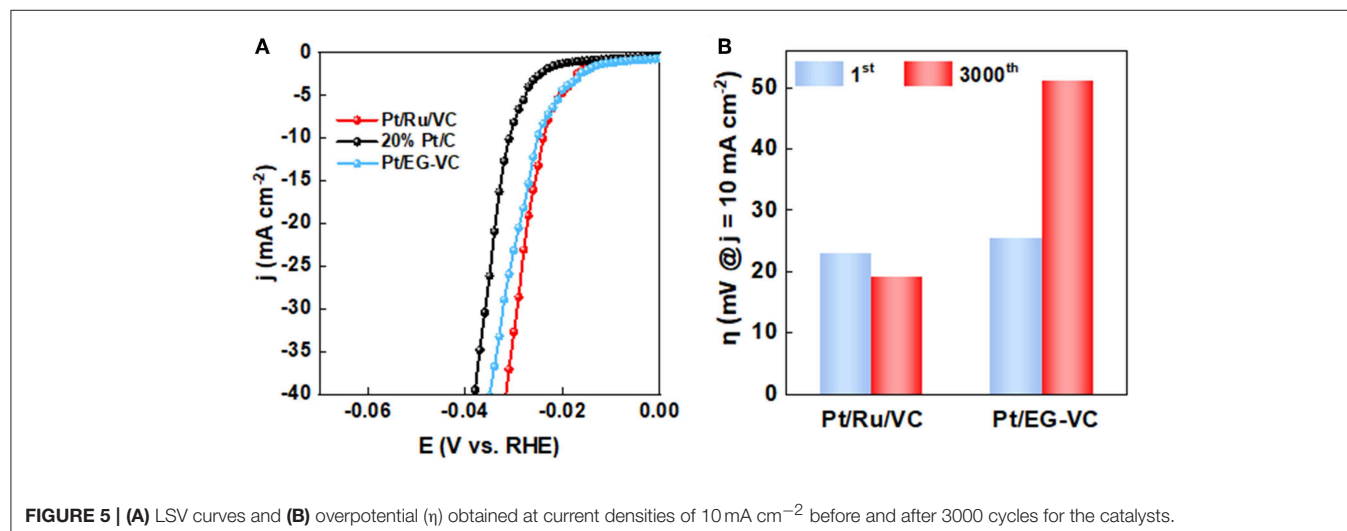


FIGURE 5 | (A) LSV curves and **(B)** overpotential (η) obtained at current densities of 10 mA cm^{-2} before and after 3000 cycles for the catalysts.

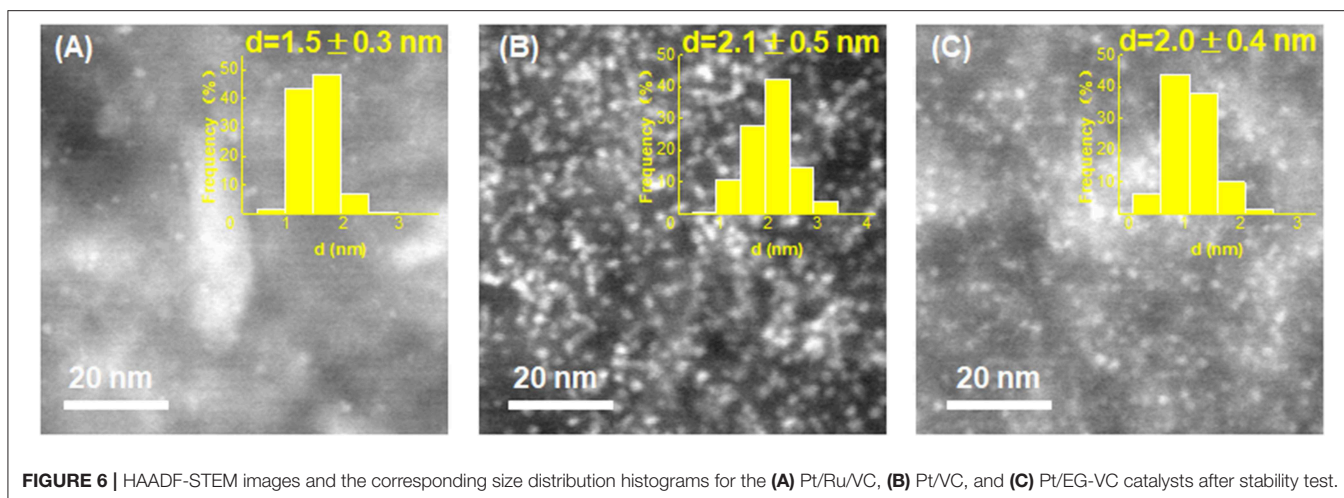


FIGURE 6 | HAADF-STEM images and the corresponding size distribution histograms for the (A) Pt/Ru/VC, (B) Pt/VC, and (C) Pt/EG-VC catalysts after stability test.

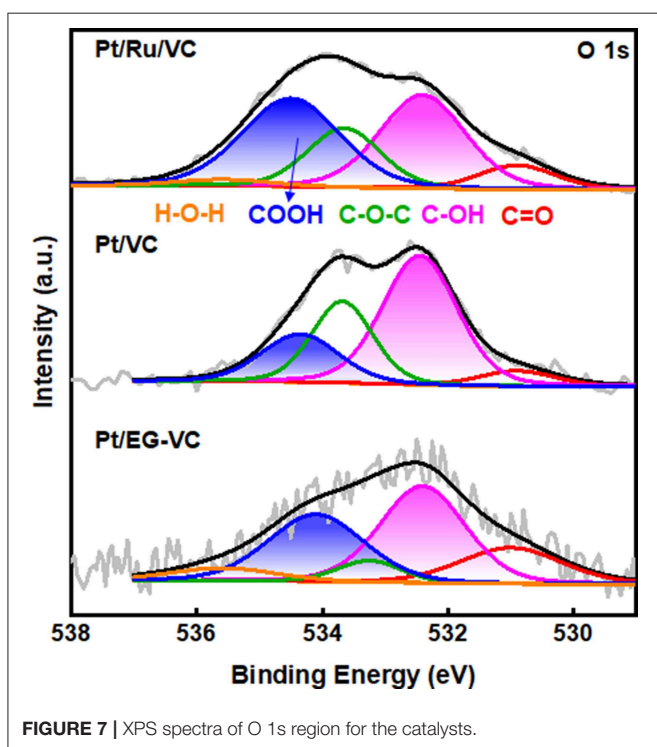


FIGURE 7 | XPS spectra of O 1s region for the catalysts.

General Discussion

Based on the above results, it could be found that functionalized VC plays a crucial role in determining the structural and electronic properties of Pt. To further investigate its influence on the catalytic performance of HER, a Ru-free catalyst was prepared according to the preparation method of the Pt/Ru/VC composite catalyst except for the addition of Ru precursor. The as-prepared catalyst was labeled as Pt/EG-VC, which was used to catalyze HER at the same conditions for a comparison. As can be seen in **Figures 5A,B**, both the HER activity and stability for the Pt/EG-VC catalyst were inferior to those of the Pt/Ru/VC

composite catalyst. Similarly, XPS was employed to characterize the electronic properties of the Pt/EG-VC composite catalyst. As shown in **Figure S2**, the Pt/EG-VC catalyst shows lower Pt⁰ 4f binding energy of 71.9 eV in comparison with that of 72.0 eV for the Pt/Ru/VC composite catalyst, consistent with the higher Pt binding energy corresponding to higher activity. Thus, from the point of view of electronic properties, the functionalized VC would increase Pt 4f binding energy toward high HER activity.

On the other hand, HAADF-STEM was employed to compare the structural properties of these catalysts before and after stability testing. As shown in **Figure 6**, both the used Pt/VC and Pt/EG-VC catalysts exhibit remarkable Pt aggregates over the catalyst surface, and the corresponding average particle sizes are determined to be 2.1 ± 0.5 and 2.0 ± 0.4 nm, respectively. The increased Pt particle size could result in the loss of Pt active sites during the test and thus lower HER stability. However, for the Pt/Ru/VC composite catalyst, it could be seen that the metal particles still remain highly distributed across catalyst surface, and the average metal particle size is determined to be 1.5 ± 0.3 nm, which is similar to that of the fresh one. Thus, from the point of view of structural properties, the functionalized VC would help stabilize metal particles in resistance of agglomeration toward high HER stability.

Based on the above results, the functionalized VC strongly affects the electronic and structural properties of Pt in terms of their catalytic performance for HER. To probe the origin of functionalization, XPS O 1s spectra for the Pt/Ru/VC, Pt/VC and Pt/EG-VC catalyst was further deconvoluted as shown in **Figure 7**. Obviously, Pt/Ru/VC has higher content of carboxyl group in comparison with the other two catalysts, which accounts for more than 37% of the total oxygen species. Previous studies (Bock et al., 2004; Fang et al., 2019) have suggested that ethylene glycol could act as the reducing reagent for metal particle, and the as-produced glycolic acid could adsorb on catalyst surface. These glycolic acids involve abundant surface functional groups, such as carboxyl groups, evidenced by the XPS O 1s spectra. As following, during the ALD process, the Pt precursor would prefer to react and substitute the surface functional groups upon O₃ treatment

(Munnik et al., 2015), thus giving rise to separate Pt particles instead of alloy.

CONCLUSION

In summary, we have successfully synthesized cost-effective Pt-based HER catalysts by the ALD technique to immobilize Pt nanoparticles on the functionalized VC. The as-synthesized Pt/Ru/VC composite catalyst exhibits more Pt active sites, desirable Pt electronic properties and high electron conductivity, giving rise to the highest HER activity compared with the referenced Pt/VC, Ru/VC and commercial 20 wt% Pt/C catalyst. Specifically, the outstanding HER activity includes the small Tafel slope of 30.6 mV dec⁻¹ as well as the comparable overpotentials (23 and 30 mV) and current densities (10 and 40 mA cm⁻²). Moreover, the Pt/Ru/VC composite catalyst exhibits excellent HER stability with almost no activity loss after 3000 cycles. The insights revealed here could guide the rational design and optimization of cost-effective carbon supported Pt-based catalysts for the HER based on the ALD technique.

DATA AVAILABILITY STATEMENT

All datasets generated for this study are included in the manuscript/**Supplementary Files**.

REFERENCES

- Anantharaj, S., Karthick, K., Venkatesh, M., Simha, T. V., Salunke, A. S., Ma, L., et al. (2017). Enhancing electrocatalytic total water splitting at few layer Pt-NiFe layered double hydroxide interfaces. *Nano Energy* 39, 30–43. doi: 10.1016/j.nanoen.2017.06.027
- Anantharaj, S., Karthik, P. E., Subramanian, B., and Kundu, S. (2016). Pt nanoparticle anchored molecular self-assemblies of DNA: an extremely stable and efficient HER electrocatalyst with ultralow Pt content. *ACS Catal.* 6, 4660–4672. doi: 10.1021/acscatal.6b00965
- Bock, C., Paquet, C., Couillard, M., Botton, G. A., and MacDougall, B. R. (2004). Size-selected synthesis of PtRu nano-catalysts: reaction and size control mechanism. *J. Am. Chem. Soc.* 126, 8028–8037. doi: 10.1021/ja0495819
- Chao, T., Luo, X., Chen, W., Jiang, B., Ge, J., Lin, Y., et al. (2017). Atomically dispersed copper-platinum dual sites alloyed with palladium nanorings catalyze the hydrogen evolution reaction. *Angew. Chem. Int. Ed.* 56, 16047–16051. doi: 10.1002/anie.201709803
- Cheng, N., Stambula, S., Wang, D., Banis, M. N., Liu, J., Riese, A., et al. (2016). Platinum single-atom and cluster catalysis of the hydrogen evolution reaction. *Nat. Commun.* 7:13638. doi: 10.1038/ncomms13638
- Dennany, L., Sherrill, P., Chen, J., Innis, P. C., Wallace, G. G., and Minett, A. I. (2010). EPR characterisation of platinum nanoparticle functionalised carbon nanotube hybrid materials. *Phys. Chem. Chem. Phys.* 12, 4135–4141. doi: 10.1039/b923921a
- Durst, J., Simon, C., Siebel, A., Rheinländer, P. J., Schuler, T., Hanzlik, M., et al. (2014). hydrogen oxidation and evolution reaction (HOR/HER) on Pt electrodes in acid vs. alkaline electrolytes: mechanism, activity and particle size effects. *ECS Trans.* 64, 1069–1080. doi: 10.1149/06403.1069ecst
- Fang, B., Chaudhari, N. K., Kim, M. S., Kim, J. H., and Yu, J. S. (2019). Homogeneous deposition of platinum nanoparticles on carbon black for proton exchange membrane fuel cell. *J. Am. Chem. Soc.* 131, 15330–15338. doi: 10.1021/ja905749e

AUTHOR CONTRIBUTIONS

WL and JG performed the catalysts preparation and characterization, electrochemical measurements, and wrote the manuscript. ZH and WC carried out TGA and XPS measurements. GQ and XZ helped to analyze the data. XD conceived the idea and wrote the paper. All authors contributed to the preparation of the manuscript.

FUNDING

This work was financially supported by the Natural Science Foundation of China (21922803 and 21776077), the Shanghai Natural Science Foundation (17ZR1407300 and 17ZR1407500), the Program for Professor of Special Appointment (Eastern Scholar) at Shanghai Institutions of Higher Learning, the Shanghai Rising-Star Program (17QA1401200), the State Key Laboratory of Organic-Inorganic Composites (oic-201801007), and the Open Project of State Key Laboratory of Chemical Engineering (SKLChE-15C03).

SUPPLEMENTARY MATERIAL

The Supplementary Material for this article can be found online at: <https://www.frontiersin.org/articles/10.3389/fmats.2019.00251/full#supplementary-material>

- Gao, Z., and Qin, Y. (2017). Design and properties of confined nanocatalysts by atomic layer deposition. *Acc. Chem. Res.* 50, 2309–2316. doi: 10.1021/acs.accounts.7b00266
- George, S. M. (2009). Atomic layer deposition: an overview. *Chem. Rev.* 110, 111–131. doi: 10.1021/cr900056b
- Gomez, R., Fernandez-Vega, A., Feliu, J. M., and Aldaz, A. (1993). Hydrogen evolution on platinum single crystal surfaces: effects of irreversibly adsorbed bismuth and antimony on hydrogen adsorption and evolution on platinum (100). *J. Phys. Chem.* 97, 4769–4776. doi: 10.1021/j100120a032
- Greeley, J., Nørskov, J. K., Kibler, L. A., El-Aziz, A. M., and Kolb, D. M. (2006). Hydrogen evolution over bimetallic systems: Understanding the trends. *ChemPhysChem* 7, 1032–1035. doi: 10.1002/cphc.200500663
- Hou, D., Zhou, W., Liu, X., Zhou, K., Xie, J., Li, G., et al. (2015). Pt nanoparticles/MoS₂ nanosheets/carbon fibers as efficient catalyst for the hydrogen evolution reaction. *Electrochim. Acta* 166, 26–31. doi: 10.1016/j.electacta.2015.03.067
- Jiang, H., Lin, Y., Chen, B., Zhang, Y., Liu, H., Duan, X., et al. (2018). Ternary interfacial superstructure enabling extraordinary hydrogen evolution electrocatalysis. *Mater. Today* 21, 602–610. doi: 10.1016/j.mattod.2018.01.033
- Kitchin, J. R., Nørskov, J. K., Barteau, M. A., and Chen, J. G. (2004). Role of strain and ligand effects in the modification of the electronic and chemical properties of bimetallic surfaces. *Phys. Rev. Lett.* 93:156801. doi: 10.1103/PhysRevLett.93.156801
- Li, J., Liang, X., King, D. M., Jiang, Y. B., and Weimer, A. W. (2010). Highly dispersed Pt nanoparticle catalyst prepared by atomic layer deposition. *Appl. Catal.* 97, 220–226. doi: 10.1016/j.apcatb.2010.04.003
- Li, J., Liu, H., Gou, W., Zhang, M., Xia, Z., Zhang, S., et al. (2019). Ethylene-glycol ligand environment facilitates highly efficient hydrogen evolution of Pt/CoP through proton concentrating and hydrogen spillover. *Energy Environ. Sci.* 12, 2298–2304. doi: 10.1039/C9EE00752K
- Li, K., Li, Y., Wang, Y., Ge, J., Liu, C., and Xing, W. (2018). Enhanced electrocatalytic performance for the hydrogen evolution reaction through surface enrichment of platinum nanoclusters alloying with ruthenium

- in situ* embedded in carbon. *Energy Environ. Sci.* 11, 1232–1239. doi: 10.1039/C8EE00402A
- Li, Y., Wang, H., Xie, L., Liang, Y., Hong, G., and Dai, H. (2011). MoS₂ nanoparticles grown on graphene: an advanced catalyst for the hydrogen evolution reaction. *J. Am. Chem. Soc.* 133, 7296–7299. doi: 10.1021/ja201269b
- Liu, C., Wang, C. C., Kei, C. C., Hsueh, Y. C., and Perng, T. P. (2009). Atomic layer deposition of platinum nanoparticles on carbon nanotubes for application in proton-exchange membrane fuel cells. *Small* 5, 1535–1538. doi: 10.1002/smll.200900278
- Lyu, F., Wang, Q., Zhu, H., Du, M., Wang, L., and Zhang, X. (2017). A host-guest approach to fabricate metallic cobalt nanoparticles embedded in silk-derived N-doped carbon fibers for efficient hydrogen evolution. *Green Energy Environ.* 2, 151–159. doi: 10.1016/j.gee.2017.01.007
- Marichy, C., Bechelany, M., and Pinna, N. (2012). Atomic layer deposition of nanostructured materials for energy and environmental applications. *Adv. Mater.* 24, 1017–1032. doi: 10.1002/adma.201104129
- Munnik, P., de Jongh, P. E., and de Jong, K. P. (2015). Recent developments in the synthesis of supported catalysts. *Chem. Rev.* 115, 6687–6718. doi: 10.1021/cr500486u
- Ouyang, C., Feng, S., Huo, J., and Wang, S. (2017). Three-dimensional hierarchical MoS₂/CoS₂ heterostructure arrays for highly efficient electrocatalytic hydrogen evolution. *Green Energy Environ.* 2, 134–141. doi: 10.1016/j.gee.2017.01.004
- Qu, Y., Chen, B., Li, Z., Duan, X., Wang, L., Lin, Y., et al. (2019). Thermal emitting strategy to synthesize atomically dispersed Pt metal sites from bulk Pt metal. *J. Am. Chem. Soc.* 141, 4505–4509. doi: 10.1021/jacs.8b09834
- Ryndin, Y. A., Hicks, R. F., Bell, A. T., and Yermakov, Y. I. (1981). Effects of metal-support interactions on the synthesis of methanol over palladium. *J. Catal.* 70, 287–297. doi: 10.1016/0021-9517(81)90341-9
- Seh, Z. W., Kibsgaard, J., Dickens, C. F., Chorkendorff, I. B., Nørskov, J. K., and Jaramillo, T. F. (2017). Combining theory and experiment in electrocatalysis: Insights into materials design. *Science* 355:eaad4998. doi: 10.1126/science.aad4998
- Sgobba, V., and Guldi, D. M. (2009). Carbon nanotubes-electronic/electrochemical properties and application for nanoelectronics and photonics. *Chem. Soc. Rev.* 38, 165–184. doi: 10.1039/B802652C
- Shi, Y., and Zhang, B. (2016). Recent advances in transition metal phosphide nanomaterials: synthesis and applications in hydrogen evolution reaction. *Chem. Soc. Rev.* 45, 1529–1541. doi: 10.1039/C5CS00434A
- Skúlason, E., Tripkovic, V., Björketun, M. E., Gudmundsdóttir, S., Karlberg, G., Rossmeisl, J., et al. (2010). Modeling the electrochemical hydrogen oxidation and evolution reactions on the basis of density functional theory calculations. *J. Phys. Chem.* 114, 18182–18197. doi: 10.1021/jp1048887
- Wang, J., Wei, Z., Mao, S., Li, H., and Wang, Y. (2018). Highly uniform Ru nanoparticles over N-doped carbon: pH and temperature-universal hydrogen release from water reduction. *Energy Environ. Sci.* 11, 800–806. doi: 10.1039/C7EE03345A
- Yin, X. P., Wang, H. J., Tang, S. F., Lu, X. L., Shu, M., Si, R., et al. (2018). Engineering the Coordination Environment of Single-Atom Platinum Anchored on Graphdiyne for Optimizing Electrocatalytic Hydrogen Evolution. *Angew. Chem. Int. Ed.* 57, 9382–9386. doi: 10.1002/anie.201804817
- Zeng, M., and Li, Y. (2015). Recent advances in heterogeneous electrocatalysts for the hydrogen evolution reaction. *J. Mater. Chem.* 3, 14942–14962. doi: 10.1039/C5TA02974K
- Zhang, J., Chen, C., Chen, S., Hu, Q., Gao, Z., Li, Y., et al. (2017). Highly dispersed Pt nanoparticles supported on carbon nanotubes produced by atomic layer deposition for hydrogen generation from hydrolysis of ammonia borane. *Catal. Sci. Technol.* 7, 322–329. doi: 10.1039/C6CY01960A
- Zheng, Y., Jiao, Y., Jaroniec, M., and Qiao, S. Z. (2015). Advancing the electrochemistry of the hydrogen-evolution reaction through combining experiment and theory. *Angew. Chem. Int. Ed.* 54, 52–65. doi: 10.1002/anie.201407031
- Zhu, Y., Chen, G., Zhong, Y., Zhou, W., and Shao, Z. (2018). Rationally designed hierarchically structured Tungsten Nitride and Nitrogen-Rich Graphene-like carbon nanocomposite as efficient hydrogen evolution electrocatalyst. *Adv. Sci.* 5:1700603. doi: 10.1002/advs.201700603
- Zhu, Y., Lin, Y., Zhang, B., Rong, J., Zong, B., and Su, D. S. (2015). Nitrogen-doped annealed nanodiamonds with varied sp²/sp³ ratio as metal-free electrocatalyst for the oxygen reduction reaction. *Chem Cat Chem* 7, 2840–2845. doi: 10.1002/cctc.201402930
- Conflict of Interest:** The authors declare that the research was conducted in the absence of any commercial or financial relationships that could be construed as a potential conflict of interest.

Copyright © 2019 Luo, Gan, Huang, Chen, Qian, Zhou and Duan. This is an open-access article distributed under the terms of the Creative Commons Attribution License (CC BY). The use, distribution or reproduction in other forums is permitted, provided the original author(s) and the copyright owner(s) are credited and that the original publication in this journal is cited, in accordance with accepted academic practice. No use, distribution or reproduction is permitted which does not comply with these terms.